

## Article

# Improved Underwater Single-Vector Acoustic DOA Estimation via Vector Convolution Preprocessing

Haitao Dong <sup>1,2,3,†</sup>, Jian Suo <sup>3,†</sup>, Zhigang Zhu <sup>1,2,\*</sup> and Siyuan Li <sup>3</sup>

<sup>1</sup> Xi'an Key Laboratory of Intelligent Spectrum Sensing and Information Fusion, Xidian University, Xi'an 710071, China; donghaitao@xidian.edu.cn

<sup>2</sup> Shaanxi Union Research Center of University and Enterprise for Intelligent Spectrum Sensing and Information Fusion, Xidian University, Xi'an 710071, China

<sup>3</sup> School of Marine Science and Technology, Northwestern Polytechnical University, Xi'an 710072, China; jiansuo@mail.nwpu.edu.cn (J.S.); li\_siyuan@mail.nwpu.edu.cn (S.L.)

\* Correspondence: zgzhuzhu@xidian.edu.cn

† These authors contributed equally to this work.

**Abstract:** Remote passive sonar detection with underwater acoustic vector sensor (UAVS) has attracted increasing attention due to its merit in measuring the full sound field information. However, the accurate estimation of the direction-of-arrival (DOA) remains a challenging problem, especially under low signal-to-noise ratio (SNR) conditions. In this paper, a novel convolution (COV)-based single-vector acoustic preprocessing method is proposed on the basis of the single-vector acoustic preprocessing model. In view of the theoretical analysis of the classical single-vector acoustic DOA estimation method, the principle of preprocessing can be described as “to achieve an improved denoising performance in the constraint of equivalent amplitude gain and phase response.” This can be naturally guaranteed by our proposed COV method. In addition, the upper bound with matched filtering (MF) preprocessing is provided in the consideration of the optimal linear signal processing for weak signal detection under Gaussian noise. Numerical analyses demonstrate the effectiveness of our proposed preprocessing method with both vector array signal processing-based and intensity-based methods. Experimental verification conducted in South China Sea further verifies the effectiveness of our approach for practical applications. This work can lay a solid foundation in improving underwater remote vector acoustic DOA estimation under low SNR, and can provide important guidance for future research work.

**Keywords:** underwater acoustic vector sensor (UAVS); direction-of-arrival (DOA) estimation; vector convolution (COV) preprocessing; low signal-to-noise ratio (SNR)



**Citation:** Dong, H.; Suo, J.; Zhu, Z.; Li, S. Improved Underwater Single-Vector Acoustic DOA Estimation via Vector Convolution Preprocessing. *Electronics* **2024**, *13*, 1796. <https://doi.org/10.3390/electronics13091796>

Academic Editors: Mário P. Véstias and Rui Policarpo Duarte

Received: 5 April 2024

Revised: 30 April 2024

Accepted: 6 May 2024

Published: 6 May 2024



**Copyright:** © 2024 by the authors. Licensee MDPI, Basel, Switzerland. This article is an open access article distributed under the terms and conditions of the Creative Commons Attribution (CC BY) license (<https://creativecommons.org/licenses/by/4.0/>).

## 1. Introduction

Direction-of-arrival (DOA) estimation is of key importance for underwater sonar applications such as coastal surveillance, target tracking, and navigation. This can be generally realized by traditional pressure sensor arrays with beamforming and time delay estimation approaches [1]. In recent years, utilizing underwater acoustic vector sensor (UAVS) has attracted an increasing attention due to its merits in measuring the full sound field information [2–4]. A single UAVS is composed of three orthogonally oriented uniaxial particle-velocity sensors plus a pressure sensor, all collocated in a point-like spatial geometry. In comparison to traditional pressure sensor arrays, acoustic vector arrays can be seen as an extended array with several times the number of array elements with the same aperture size, hence overcoming the disadvantages of conventional arrays with large aperture size. Moreover, they can estimate both elevation and azimuth without left–right ambiguity [5–10].

A single UAVS can be regarded as a  $4 \times 1$  point space array. They have been ubiquitously applied in small underwater platforms such as gliders, ocean bottom seismome-

ters(OBS), sub-sea latent buoys, and other ocean monitoring equipment [11–14]. As a consequence, in recent years a sizable literature has focused on the applications of single UAVS, mainly for vector acoustic DOA estimation [4,5,15–23]. From the view of methodology, the single-vector acoustic DOA estimation methods can be classified into array signal processing-based and intensity-based methods. In this way, classical array signal processing-based techniques such as conventional beam forming (CBF), minimum variance distortionless response (MVDR), estimation of signal parameters via the rotational invariance technique (ESPRIT), multiple signal characteristic (MUSIC), and others can be initially adopted in the consideration of a point space array [15–17,24]. However, the different signal-to-noise ratios (SNRs) of the vector channels may corrupt the signal subspace, leading to the performance degradation when using the method under low-SNR circumstances. To ease the influence of noise, several research works have adopted denoising preprocessing methods to improve estimation performance. Agarwal et al. [25] employed higher-order statistics for preprocessing, which can increase the sound source count estimation when utilizing a single UAVS. Zhang et al. [26] considered the Gaussian noise suppression characteristic of higher-order cumulants and proposed a high-resolution ESPRIT algorithm for single UAVS DOA estimation, which can improve the estimation accuracy at lower SNR. Intensity-based methods can generally be classified into two major categories: average acoustic intensity measurement (AAIM)-based methods in the time domain, and complex acoustic intensity measurement (CAIM)-based methods in the frequency domain [5]. Related research has been ongoing for a long time. Experimental comparisons and verifications have shown that CAIM-based methods have more potential in comparison with array signal processing-based and intensity-based methods [16]. As acoustic intensity measurement-based algorithms are proposed for zero mean and uncorrelated background noise, these methods are generally limited to higher SNR conditions and ideal white Gaussian noise (WGN) backgrounds. Therefore, for practical applications, the CAIM method suffers from low accuracy, especially for remote targets corresponding to lower SNR and complex ocean ambient noise conditions. To ease this problem, a weighted bar graph statistics-based CAIM method named WCAIM has been proven to obtain better vector acoustic DOA estimation performance [16]. Zhong et al. [27] utilized the particle filtering approach for vector acoustic DOA estimation, resulting in improved accuracy and performance for tracking processing. Similarly, Gunes et al. [28] utilized a Bernoulli filter and random finite sets to reprocess the vector acoustic DOA estimations for better tracking. Chen et al. [29] proposed a source counting method of vector acoustic DOA histograms for distinguishing multiple sources. This can certainly improve the estimation performance due to its statistical property; however, it is essentially unable to solve the low SNR problem, as it is a postprocessing approach. Such methods, which reprocess the DOA estimation outputs within a period of time to decrease the estimation error can be regarded as postprocessing; however, these postprocessing methods are essentially unable to solve the issue of poor accuracy under low SNR conditions. Thus, several researchers have focused on preprocessing approaches. Zhao et al. [18] proposed an improved vector DOA estimation method utilizing matched filter preprocessing, which is considered to achieve the best output under WGN background. However, this method can only be utilized with strictly prior information in active sonar systems. Stinco et al. [4] considered a modulation analysis to determine the signatures of broadband propeller cavitation noise and proposed XC-DEMON and TF-DEMON to represent the intensity vector with DEMON preprocessing. Nevertheless, while DEMON preprocessing can improve the clarification of ship features, it is invalid for processing the received signal under low SNR conditions. Machine learning has been adopted to improve single-vector acoustic DOA estimation. Wang et al. [30] proposed learning a soft mask with DNN and DNN-SVM for multi-speaker vector acoustic DOA estimation. This method can accurately extract TD-TFPs under different background noise and reverberant conditions; however, this method was developed to solve the problem under high SNR conditions. Cao et al. [31] proposed a deep transfer learning method for underwater direction-of-arrival using one UAVS, revealing the effectiveness of deep

leaning in improving the estimation accuracy. Nevertheless, the limited measured underwater sample data restricts generalization performance for real applications. In our previous work, we presented a parameter tuning method with a classical bistable stochastic resonance model for vector acoustic DOA estimation, which can effectively improve vector acoustic estimation performance under low SNR conditions [21]. This work has preliminarily demonstrated that a linear amplitude response with fixed phase shift is required for vector acoustic preprocessing; we further employed a single potential parameter tuning method for nonlinear bistable stochastic resonance to achieve a linear output response.

In view of the above analyses, while vector postprocessing methods can improve estimation performance, they are essentially unable to solve the issue of poor accuracy under low SNR conditions. To solve the problem of low SNR vector acoustic DOA estimation, vector acoustic preprocessing with noise suppression performance should be adopted. In this paper, a vector convolution-based preprocessing method is proposed on the basis of the single-vector acoustic preprocessing model to improve the performance of underwater single-vector acoustic DOA estimation. The main contributions of this work can be summarized as follows:

- (1) A single-vector acoustic preprocessing model is presented and theoretically analyzed with classical the CAIM method for a single UAVS, with the goal described as “to achieve improved denoising performance in the constraint of equivalent amplitude gain and phase response.”
- (2) A novel convolution (COV)-based single-vector acoustic preprocessing method is proposed which can naturally guarantee the linear gain-phase restrictions and achieve effective denoising performance. In addition, its upper bound with matched filtering (MF) preprocessing is provided under consideration of the optimal linear signal processing for weak signal detection under Gaussian noise.
- (3) Improved vector acoustic DOA estimation performance is achieved for both array signal processing-based and intensity-based methods. This is verified by simulation and experimental results conducted in the South China Sea.
- (4) This work can lay a solid foundation in improving underwater remote vector acoustic DOA estimation under low SNR, and can provide important guidance for future research work.

The rest of the paper is arranged as follows. In Section 2, the signal model and three classical single vector acoustic DOA estimation approaches are provided and compared with the mean error (ME) and root mean square error (RMSE). In Section 3, the single-vector acoustic preprocessing model is presented and theoretically analyzed with the classical UAVS CAIM method, and the detailed implementation of the proposed convolution (COV)-based single vector acoustic preprocessing method is further described. Simulation results are evaluated in Section 4, and experimental verification conducted in the South China Sea is further discussed in Section 5. Finally, concluding remarks are drawn in Section 6.

## 2. Single-Vector Acoustic DOA Estimation Model

### 2.1. Signal Model

An “underwater acoustic vector sensor” (UAVS) (known as an “underwater vector hydrophone”) is composed of three orthogonally oriented uniaxial particle-velocity sensors plus a pressure sensor in a point-like spatial geometry. It is composed of a sound pressure sensor and vibration speed sensor that measure the pressure and the vibration velocity of the sound field at one point. Located at the origin of the Cartesian coordinate system, at any time  $t$  it measures the sound pressure  $p(t)$  and three orthogonal components represented as  $v_x(t)$ ,  $v_y(t)$ , and  $v_z(t)$  along the  $x$ -,  $y$ -, and  $z$ - axes, respectively.

For simplicity, in the following discussion we assume plane waves  $x$ ,  $o$ ,  $y$  and a source

signal  $s(t)$  while omitting the height information. The observations of the AVS can be expressed as [22]

$$\mathbf{y}(t) = \begin{bmatrix} p(t) \\ v_x(t) \\ v_y(t) \end{bmatrix} = \begin{bmatrix} s(t) \\ \frac{1}{\rho c_0} s(t) \cos \theta \sin \alpha \\ \frac{1}{\rho c_0} s(t) \sin \theta \sin \alpha \end{bmatrix} + \begin{bmatrix} n_p(t) \\ n_x(t) \\ n_y(t) \end{bmatrix} \quad (1)$$

where  $s(t)$  is the source signal,  $\rho$  and  $c_0$  are the density and velocity of the sound of water,  $\alpha \in (0, \pi]$  symbolizes the incident elevation angle of the source measured from the positive  $z$ -axis, and  $\theta \in (0, 2\pi]$  denotes the corresponding azimuth angle measured from the positive  $x$ -axis. Assuming that the vector sensor is far away from the sound source, the signal arriving at the vector hydrophone can be regarded as a plane wave. For this circumstance,  $n_p(t)$ ,  $n_x(t)$ , and  $n_y(t)$  are the corresponded noise items and are assumed to be isotropic and uncorrelated to the received source signal. Assuming that the noise field of the marine environment is isotropic, the autocorrelation coefficient of the vibration velocity channel noise is  $1/2$ ; hence, the covariance matrix  $\mathbf{R}_n$  can be expressed as [32]

$$\mathbf{R}_n = \sigma_n^2 \begin{bmatrix} 1 & 0 & 0 \\ 0 & 1/2 & 0 \\ 0 & 0 & 1/2 \end{bmatrix} \quad (2)$$

where  $\sigma_n^2$  is the variance of the  $P$  channel.

For the source signal, ship-radiated noise can be modeled as a combination of broadband noise and sinusoidal tonal signals. These sinusoidal tonals are commonly considered to be the “acoustic fingerprint” of a moving vessel (refer to ship-radiated line spectral signatures [33]). For simplicity, we can assume that the target signal consists of sinusoidal tonals, as below:

$$s(t) = \sum_{i=1}^k A_i e^{j2\pi f_i t + \varphi_i} \quad (3)$$

where  $k$  is the number of ship-radiated line spectral signatures,  $f_i$  represents the character frequencies, and  $A_i$  and  $\varphi_i$  are the corresponding amplitudes and phases, respectively. Note that the velocity direction characteristics of UAVS are frequency-independent.

## 2.2. Classical Single-Vector Acoustic DOA Estimation Approaches

In this paper, three classical single-vector acoustic DOA estimation approaches are adopted to better reveal the performance and generalizability of our proposed method for both array signal processing-based methods (MUSIC) and intensity-based methods (AAIM and CAIM).

### 2.2.1. MUSIC for UAVS

A single vector hydrophone can be described as a special point space array, and its array manifold vector can be represented as

$$A_k(\theta) = [ 1 \quad \sin \alpha \cos \theta \quad \sin \alpha \sin \theta ]^T. \quad (4)$$

On this basis, general array signal processing methods can be introduced to achieve azimuthal estimation of targets. Here, the classical MUSIC algorithm is adopted over other array signal processing methods due to its high resolution and accuracy. Its spatial spectrum output can be provided by

$$\hat{P}(\theta) = \frac{1}{A_k^H \mathbf{U}_n \mathbf{U}_n^H A_k} = \frac{1}{A_k^H (I - \mathbf{U}_s \mathbf{U}_s^H) A_k} \quad (5)$$

where  $U_s$  and  $U_n$  represent the signal subspace and noise subspace, respectively, while  $I$  is the identity matrix.

### 2.2.2. AAIM for UAVS

The intensity-based azimuth  $\theta$  estimation with average acoustic intensity can be calculated as follows:

$$\mathbf{I} = [I_{px}, I_{py}]^T = \langle p(t) \cdot \mathbf{v}(t) \rangle \quad (6)$$

where  $\langle \cdot \rangle$  denotes time averaging and  $\mathbf{v}(t) = [v_x(t), v_y(t)]$  stands for the vibration velocity of channels  $x$  and  $y$ ; the corresponding  $I_{px}$  and  $I_{py}$  can be obtained by

$$\begin{aligned} I_{px} &= \langle p(t)v_x(t) \rangle \\ I_{py} &= \langle p(t)v_y(t) \rangle \end{aligned} \quad (7)$$

meaning that the intensity-based azimuth estimator can be provided as follows:

$$\hat{\theta} = \arctan \frac{I_{py}}{I_{px}} \quad (8)$$

where  $\hat{\theta}$  is the estimation of the target azimuth angle.

### 2.2.3. CAIM for UAVS

Such a calculation can be completed in the frequency domain or time–frequency domain with complex conjugating and the complex acoustic intensity measurement (CAIM) algorithm [16]. Due to the sparse nature of the target signal energy in the frequency domain, using CAIM can achieve a frequency domain filtering effect. As it can more accurately and effectively distinguish multiple targets with different line spectra signatures, CAIM performs better than AAIM, especially under low SNR and multi-target-source conditions. The direction of the intensity can be obtained by,

$$\mathbf{S}(\omega) = [S_{px}(\omega), S_{py}(\omega)]^T = [P(\omega)V_x^*(\omega), P(\omega)V_y^*(\omega)] \quad (9)$$

where  $P(\omega)$ ,  $V_x(\omega)$ , and  $V_y(\omega)$  are the Fourier transforms of  $p(t)$ ,  $v_x(t)$ ,  $v_y(t)$ , respectively, while  $X^*$  denotes the complex conjugating

$$\hat{\theta}(\omega) = \arctan \frac{\Re(S_{py}(\omega))}{\Re(S_{px}(\omega))} = \arctan \frac{\Re(P(\omega)V_y^*(\omega))}{\Re(P(\omega)V_x^*(\omega))} \quad (10)$$

where  $\hat{\theta}(\omega)$  represents the estimated azimuth angle corresponding to a frequency bin and  $\Re(\cdot)$  represents the real part.

A simulated comparison of these three vector acoustic DOA estimation methods is provided in Figure 1. The target source azimuth is simulated as  $30^\circ$  with a single line spectrum  $f_i = 100$  Hz, then the mean error (ME) and root mean square error (RMSE) of the azimuth angle are evaluated, where it can be seen that CAIM performs the best. The corresponding ME and RMSE are defined as follows:

$$\text{ME} = \left| \frac{1}{N} \sum_{i=1}^N (\theta - \hat{\theta}) \right| \quad (11)$$

and

$$\text{RMSE} = \sqrt{\frac{1}{N} \sum_{i=1}^N (\theta - \hat{\theta})^2} \quad (12)$$

where  $\theta$  and  $\hat{\theta}$  represent the true azimuth and estimated azimuth of the source, respectively, while  $N$  is the number of independent Monte Carlo trials. Note that every data point here is obtained by 1000 independent realizations. In this paper, the SNR is defined as follows:

$$\text{SNR} = 10\log_{10} \frac{P(\omega_k)}{\sum_{i=1}^{N/2} P(\omega_i) - P(\omega_k)} \tag{13}$$

where  $P(\omega_k)$  represents the energy of signal  $s(t)$  with a single frequency  $\omega_k$ ,  $N$  is the length of the discrete Fourier transform (DFT) number, and the item  $\sum_{i=1}^{N/2} P(\omega_i) - P(\omega_0)$  is the total energy of the background noise. Note that in the rest of this paper, the SNR is calculated by channel P.

As shown in Figure 1a, CAIM can perform better than AAIM and MUSIC, especially under low SNR conditions. This indicates improved performance for CAIM with postprocessing approaches such as vector acoustic DOA histogram, particle filtering approaches, etc. The RMSE comparison in Figure 1b is in accordance with the above analysis, indicating that CAIM is superior in practical situations with SNR > -20 dB. Nevertheless, under circumstances where SNR < -20 dB, the RMSE of CAIM is worse than that of AAIM. In fact, all three methods see decreased performance with large estimation errors. The AAIM results tend towards 30° as a constant, with the background noise taking a dominant position. Note that 2° and 5° reference lines are utilized to provide guidance for practical applications.

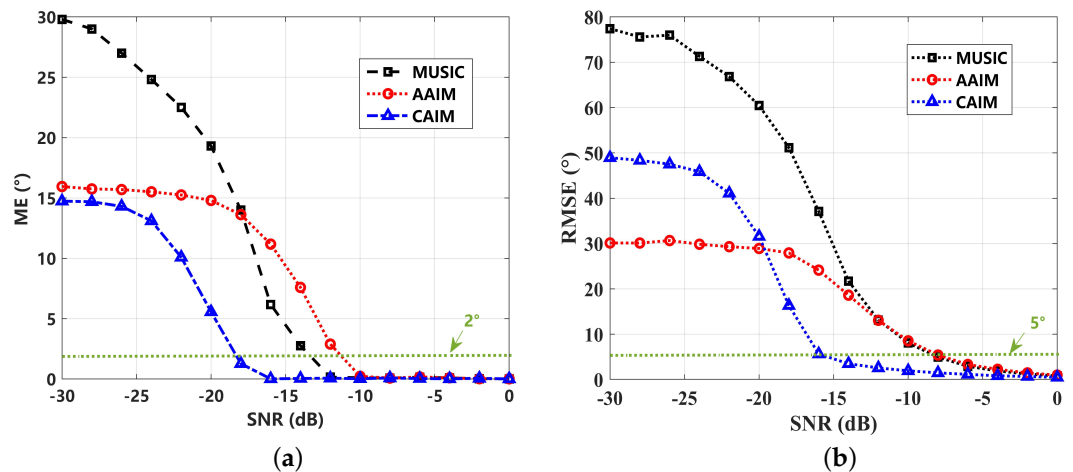


Figure 1. Performance comparison of three vector acoustic DOA estimation methods in terms of (a) mean error (ME) and (b) root mean square error (RMSE).

### 3. Method

#### 3.1. Single-Vector Acoustic Preprocessing Model

In general, to improve vector acoustic DOA estimation performance, signal preprocessing with noise reduction methods should be adopted, especially under low SNR conditions. However, different methods will result in different amplitude gains and random phase lag responses, potentially causing unexpected and significant estimation errors.

To analyze the factors influencing estimation accuracy with general preprocessing (or noise reduction) methods, a generalized vector acoustic preprocessing analysis model is provided below. The denoised vector signal  $y'(t)$  can be subjected to the non-ideal gain-phase responses in order to generate an amplitude gain  $G$  and random phase lag  $\varphi$ , as follows:

$$y'(t) = \begin{bmatrix} p'(t) \\ v'_x(t) \\ v'_y(t) \end{bmatrix} = \begin{bmatrix} G_p(\omega)e^{j\varphi_p(\omega)}s(t) + n'_p(t) \\ \frac{G_x(\omega)}{\rho c_0}e^{j\varphi_x(\omega)}s(t)\cos\theta\sin\alpha + n'_x(t) \\ \frac{G_y(\omega)}{\rho c_0}e^{j\varphi_y(\omega)}s(t)\sin\theta\sin\alpha + n'_y(t) \end{bmatrix} \quad (14)$$

where  $G_p(\omega)$ ,  $G_x(\omega)$ ,  $G_y(\omega)$  denote the amplitude gain response of the components of the pressure sensor and the uniaxial velocity sensor oriented along the  $x$ -axis and  $y$ -axis, respectively, while  $\varphi_p(\omega)$ ,  $\varphi_x(\omega)$ ,  $\varphi_y(\omega)$  represent the corresponding phase bias response, which can be modeled as a stochastic and arbitrary distribution. Finally,  $n'_p(t)$ ,  $n'_x(t)$ ,  $n'_y(t)$  represent the preprocessed noise items and generalized assumed certain correlation with nonzero mean. Note that  $G_p(\omega) = G_x(\omega) = G_y(\omega) = 1$ ,  $\varphi_p(\omega) = \varphi_x(\omega) = \varphi_y(\omega) = 0$ , and there is no pretreatment, which is consistent with the received signal of Equation (1).

In the consideration of preprocessing, we neglecting  $\rho c_0$ , meaning that we have the intensity of CAIM for the UAVS denoised vector signal  $y'(t)$ , as follows:

$$\begin{cases} P'(\omega) = \pi G_p(\omega) A_s(\omega) [\delta(\omega + \omega_0) e^{-j(\varphi_p(\omega) + \varphi(\omega))} + \delta(\omega - \omega_0) e^{j(\varphi_p(\omega) + \varphi(\omega))}] + N_p(\omega) \\ V'_x(\omega) = \pi G_x(\omega) A_s(\omega) [\delta(\omega + \omega_0) e^{-j(\varphi_x(\omega) + \varphi(\omega))} + \delta(\omega - \omega_0) e^{j(\varphi_x(\omega) + \varphi(\omega))}] \cos\theta \cos\alpha + N_x(\omega) \\ V'_y(\omega) = \pi G_y(\omega) A_s(\omega) [\delta(\omega + \omega_0) e^{-j(\varphi_y(\omega) + \varphi(\omega))} + \delta(\omega - \omega_0) e^{j(\varphi_y(\omega) + \varphi(\omega))}] \sin\theta \cos\alpha + N_y(\omega) \end{cases} \quad (15)$$

where  $\omega = 2\pi f$  and  $\omega_0 = 2\pi f_0$  are the angular frequency,  $N_p(\omega)$ ,  $N_x(\omega)$ , and  $N_y(\omega)$  are the energy of noise corresponding to the frequency domain, and  $A_s(\omega)$  is the amplitude of signal  $s(t)$  in the frequency domain. Then, we have

$$\hat{\theta}(\omega) = \arctan \left[ \frac{\Re\{P'(\omega)V'_y{}^*(\omega)\}}{\Re\{P'(\omega)V'_x{}^*(\omega)\}} \right] \quad (16)$$

where  $\hat{\theta}(\omega)$  represents the estimated azimuth angle corresponding to the frequency bin of the target signal.

Taking the complex conjugation of  $V'_x(\omega)$  and  $V'_y(\omega)$  and multiplying with  $P'(\omega)$ , respectively,

$$\begin{cases} P'(\omega)V'_x{}^*(\omega) = F_x(\omega) \cos\theta \cos\alpha + \Delta'_x(\omega) \\ P'(\omega)V'_y{}^*(\omega) = F_y(\omega) \cos\theta \cos\alpha + \Delta'_y(\omega) \end{cases} \quad (17)$$

in which  $F_x(\omega)$ ,  $F_y(\omega)$ ,  $\Delta'_x(\omega)$ , and  $\Delta'_y(\omega)$  can be written as

$$\begin{cases} F_x(\omega) = \pi^2 G_p(\omega) G_x^*(\omega) A_s^2(\omega) [\delta^2(\omega + \omega_0) e^{j(\varphi_x(\omega) - \varphi_p(\omega))} + \delta^2(\omega - \omega_0) e^{j(\varphi_p(\omega) - \varphi_x(\omega))}] \\ \quad + N_p(\omega) \pi G_x^*(\omega) A_s^*(\omega) [\delta(\omega + \omega_0) e^{-j(\varphi_x(\omega) + \varphi(\omega))} + \delta(\omega - \omega_0) e^{j(\varphi_x(\omega) + \varphi(\omega))}] \\ F_y(\omega) = \pi^2 G_p(\omega) G_y^*(\omega) A_s^2(\omega) [\delta^2(\omega + \omega_0) e^{j(\varphi_y(\omega) - \varphi_p(\omega))} + \delta^2(\omega - \omega_0) e^{j(\varphi_p(\omega) - \varphi_y(\omega))}] \\ \quad + N_p(\omega) \pi G_y^*(\omega) A_s^*(\omega) [\delta(\omega + \omega_0) e^{-j(\varphi_y(\omega) + \varphi(\omega))} + \delta(\omega - \omega_0) e^{j(\varphi_y(\omega) + \varphi(\omega))}] \end{cases} \quad (18)$$

and

$$\begin{cases} \Delta'_x(\omega) = N_x^*(\omega) \pi G_p(\omega) A_s(\omega) [\delta(\omega + \omega_0) e^{-j(\varphi_p(\omega) + \varphi(\omega))} + \delta(\omega - \omega_0) e^{j(\varphi_p(\omega) + \varphi(\omega))}] + N_p(\omega) N_x^*(\omega) \\ \Delta'_y(\omega) = N_y^*(\omega) \pi G_p(\omega) A_s(\omega) [\delta(\omega + \omega_0) e^{-j(\varphi_p(\omega) + \varphi(\omega))} + \delta(\omega - \omega_0) e^{j(\varphi_p(\omega) + \varphi(\omega))}] + N_p(\omega) N_y^*(\omega) \end{cases} \quad (19)$$

where  $\delta(\omega + \omega_0)\delta(\omega - \omega_0) = 0$ .

Expanding Equations (18) and (19) using Euler's formula and taking the real part, we have

$$\begin{cases} \Re[F_x(\omega)] = 2[\pi^2 \Re[G_p(\omega) G_x^*(\omega)] A_s^2(\omega) \delta^2(\omega - \omega_0) + \Re[N_p(\omega) \pi G_x^*(\omega) A_s^*(\omega)] \delta(\omega - \omega_0)] \cos(\varphi_x(\omega) - \varphi_p(\omega)) \\ \Re[F_y(\omega)] = 2[\pi^2 \Re[G_p(\omega) G_y^*(\omega)] A_s^2(\omega) \delta^2(\omega - \omega_0) + \Re[N_p(\omega) \pi G_y^*(\omega) A_s^*(\omega)] \delta(\omega - \omega_0)] \cos(\varphi_y(\omega) - \varphi_p(\omega)) \end{cases} \quad (20)$$

and

$$\begin{cases} \Re[\Delta'_x(\omega)] = 2\Re[N_x^*(\omega)\pi G_p(\omega)A_s(\omega)]\delta(\omega - \omega_0) \cos(\varphi_x(\omega) - \varphi_p(\omega)) + \Re[N_p(\omega)N_x^*(\omega)] \\ \Re[\Delta'_y(\omega)] = 2\Re[N_y^*(\omega)\pi G_p(\omega)A_s(\omega)]\delta(\omega - \omega_0) \cos(\varphi_y(\omega) - \varphi_p(\omega)) + \Re[N_p(\omega)N_y^*(\omega)] \end{cases} \quad (21)$$

Its asymptotic unbiased estimator  $\hat{\theta}'$  can be obtained as shown below.

$$\begin{aligned} \hat{\theta}'(\omega_0) &= \arctan\left\{\frac{\Re[P'(\omega_0)V_y'^*(\omega_0)]}{\Re[P'(\omega_0)V_x'^*(\omega_0)]}\right\} \\ \text{s.t.} \quad &\Re[F_x(\omega_0)] \equiv \Re[F_y(\omega_0)] \\ &\Re[\Delta'_x(\omega_0)] \rightarrow 0 \\ &\Re[\Delta'_y(\omega_0)] \rightarrow 0 \end{aligned} \quad (22)$$

In view of this, the constraints can be discussed as follows:

(1) For the first constraint  $\Re[F_x(\omega_0)] \equiv \Re[F_y(\omega_0)]$ , according to the Equation (20), we can see that its amplitude is directly related to the amplitude gain response  $G_p(\omega)$ ,  $G_x(\omega)$ ,  $G_y(\omega)$  and phase bias response  $\varphi_p$ ,  $\varphi_x$ ,  $\varphi_y$ . In the strict sense, we can find a particular solution with equivalent amplitude gain responses as well as phase bias lags, that is to say,

$$\begin{cases} G_p(\omega) = G_x(\omega) = G_y(\omega) \\ \varphi_p(\omega) = \varphi_x(\omega) = \varphi_y(\omega) \end{cases} \quad (23)$$

(2) To asymptotically achieve  $\Re[\Delta'_x(\omega_0)] \rightarrow 0$  and  $\Re[\Delta'_y(\omega_0)] \rightarrow 0$ , preprocessing approaches should have a filtering effect that can enhance the signal-to-noise ratio improvement (SNRI) performance of the vector channels. The SNRI is generally utilized to evaluate the filtering performance for input and output signals [34]. In the consideration of low-SNR conditions, noise reduction performance should be addressed in the signal preprocessing approach.

In view of this, Equation (22) can be eased and rewritten as follows:

$$\begin{aligned} \hat{\theta}' &= \arctan\left\{\frac{\Re[P'(\omega_0)V_y'^*(\omega_0)]}{\Re[P'(\omega_0)V_x'^*(\omega_0)]}\right\} \\ \text{s.t.} \quad &G_x(\omega) = G_y(\omega) \\ &\varphi_x(\omega) = \varphi_y(\omega) \\ &\text{SNRI} \geq 1 \end{aligned} \quad (24)$$

where  $\text{SNRI} \geq 1$  is to guarantee the required noise reduction performance. The goal of this model can be described as "to achieve an improved denoising performance in the constraint of equivalent amplitude gain and phase response."

### 3.2. Convolution (COV)-Based Single-Vector Acoustic Preprocessing

Convolution (also known as linear convolution) is an operation that describes the relationship between the input and output of a linear system in the time domain. Considering its linear property, it is naturally suitable for vector acoustic preprocessing.

The convolution of two signals can be accomplished as follows:

$$f_1(t) * f_2(t) = \int_{-\infty}^{\infty} f_1(t)f_2(t - \tau) \quad (25)$$

where  $*$  represents the convolution operator. According to the time domain convolution theorem, the convolution integral of two signals in the time domain corresponds to the product of their Fourier transforms in the frequency domain, as follows:

$$F[f_1(t) * f_2(t)] = F_1(\omega)F_2(\omega) \quad (26)$$

where  $F$  is the Fourier transform operator and  $F_1(\omega)$  and  $F_2(\omega)$  are the Fourier transforms of  $f_1(t)$  and  $f_2(t)$ , respectively.

Assuming that channel  $p$  is adopted for convolution preprocessing, we have the output of three channels  $p'(t)$ ,  $v'_x(t)$ ,  $v'_y(t)$ , as follows:

$$\begin{cases} p'(t) = p(t) * p(t) \\ v'_x(t) = v_x(t) * p(t) \\ v'_y(t) = v_y(t) * p(t) \end{cases} \quad (27)$$

Then, we have the Fourier transform

$$\begin{cases} P'(\omega) = P(\omega)P(\omega) \\ V'_x(\omega) = V_x(\omega)P(\omega) \\ V'_y(\omega) = V_y(\omega)P(\omega) \end{cases} \quad (28)$$

In considering the CAIM method, the complex acoustic intensity of the convolution preprocessed signals can be obtained by

$$\begin{cases} S'_{px}(\omega) = P(\omega)P(\omega)V_x^*(\omega)P^*(\omega) \\ S'_{py}(\omega) = P(\omega)P(\omega)V_y^*(\omega)P^*(\omega) \end{cases} \quad (29)$$

and the azimuth estimation corresponding to  $\omega$  can be provided as

$$\hat{\theta}'(\omega) = \arctan \frac{\Re(S'_{py}(\omega))}{\Re(S'_{px}(\omega))} = \arctan \frac{\Re(P(\omega)P^*(\omega)P(\omega)V_y^*(\omega))}{\Re(P(\omega)P^*(\omega)P(\omega)V_x^*(\omega))} \quad (30)$$

where  $\hat{\theta}'(\omega)$  represents the estimated azimuth angle with convolution preprocessing. As the convolution involves linear signal processing, there is no change in the amplitude gain responses or phase bias lags. This means that the constraint in Equation (24) can be well satisfied. Then, if the constraint of  $\text{SNRI} \geq 1$  can be satisfied, the vector acoustic DOA estimation performance can be improved.

The framework of the proposed convolution-based single-vector acoustic preprocessing method for vector acoustic DOA estimation is shown in Figure 2. By adding a convolutional preprocessing module, it is possible to improve the vector acoustic DOA estimation performance. For convenience of expression, we use a simple representation of "COV" in the remainder of this paper. A detailed analysis of this module is provided below.

### (1) Selection of the reference channels.

In the following analysis, the  $p$  channel is adopted for convolution preprocessing. As is known, three signal channels  $p$ ,  $v_x$ , and  $v_y$  are measured by a UAVS. Without loss of generality, either  $v_x$  or  $v_y$  can be the reference channel. According to the signal model of UAVS, when the target azimuth is  $\theta_0$ , the projection intensity coefficient vector of its signal part on the  $x$  and  $y$  axes is  $\mathbf{A} = [\cos \theta_0, \sin \theta_0]^T$ . Due to the unknown target situation in practice, its orientation has uncertainty within the range of  $(-\pi, \pi]$ . For a certain distance of the target, the received signal-to-noise ratio of the UAVS  $p$  channel is only related to the target distance, while the signal-to-noise ratio of the  $v_x$  and  $v_y$  channels fluctuates greatly with changes in target orientation. As the  $p$  channel is omnidirectional scalar, we take the SNR received by the  $p$  channel as a reference of 0 dB. Then, a theoretical comparison of the SNR changes for channels  $v_x$  and  $v_y$  is provided as shown in Figure 3. It is clear to see that when there is a dynamic change in the SNR received by each channel, especially when the target azimuth  $\theta_0$  is close to  $0^\circ$  and  $90^\circ$ , the corresponding SNR of channels  $v_y$  and  $v_x$  is greatly decreased. This can provide guidance in the selection of reference channels, as the vector channel SNR is related to the target azimuth  $\theta_0$ . Note that the results in Figure 3 are a qualitative description according to Equation (1) and Equation (2).

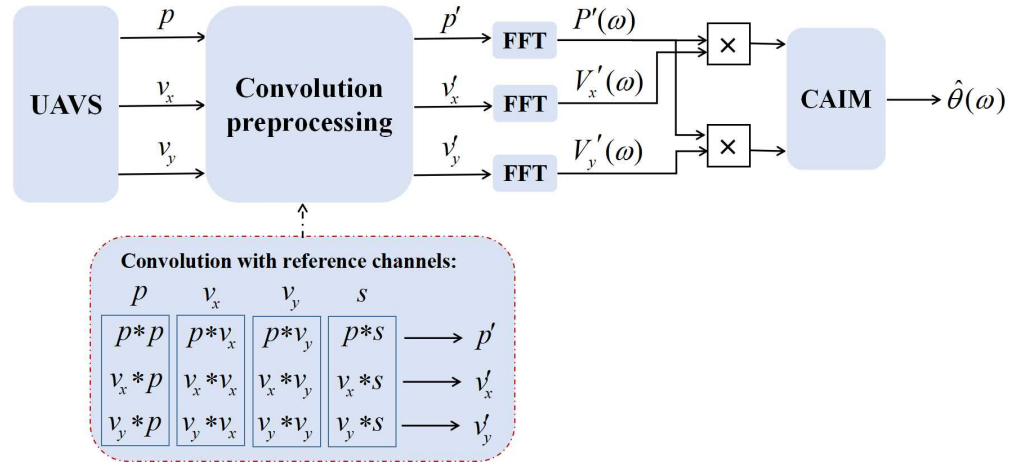


Figure 2. The framework of the proposed convolution-based single-vector acoustic preprocessing method for CAIM vector acoustic DOA estimation.

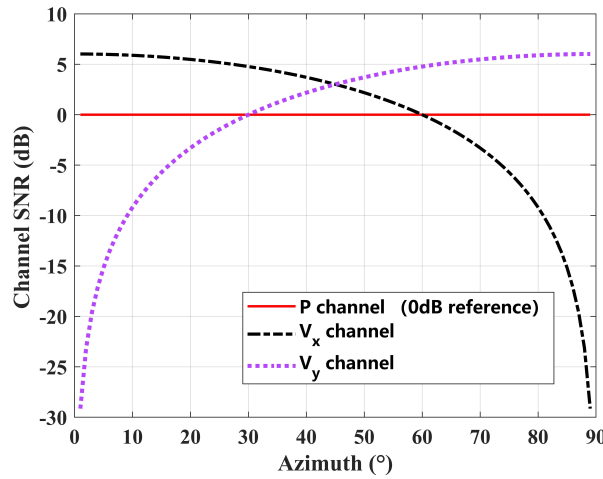


Figure 3. Comparison of differences in the received SNR of different UAVS channels when the target is at different azimuth angles.

(2) Matched filtering (MF) preprocessing with reference signal  $s(t)$ .

If the source signal  $s(t)$  is known with prior information, then the convolution-based preprocessing method is equivalent to matched filtering preprocessing. For convenience, “MF” is utilized in the rest of this paper. As we know that matched filtering is the optimal linear signal processing for weak signal detection under Gaussian noise, it should be the upper bound of the convolution-based single-vector acoustic preprocessing method, where the pure signal  $s(t)$  is utilized without any noise. The azimuth estimation corresponding to  $\omega$  can be provided as follows:

$$\hat{\theta}'_{MF}(\omega) = \arctan \frac{\Re(P(\omega)V_y^*(\omega)S^*(\omega)S(\omega))}{\Re(P(\omega)V_x^*(\omega)S^*(\omega)S(\omega))} \tag{31}$$

where  $S(\omega)$  is the Fourier transform of  $s(t)$ . Note that the matched filtering is optimal, while we need the prior knowledge of received signal frequency and phase. This prior knowledge can be acquired by active sonar systems, while it cannot be achieved for passive sonar systems. For a sonar system with a passive mode, convolution-based preprocessing can be adopted without any prior knowledge. According to Equations (30) and (31), the computational complexity of these two methods remains equal in theory.

#### 4. Analysis of Simulation Results

To evaluate and verify the performance of the proposed method, simulation and experimental results were analyzed. In view of the constraint of  $\text{SNRI} \geq 1$ , we first analyze the noise reduction performance, then the vector DOA estimation performance under different SNR conditions, which can verify the effectiveness of convolution preprocessing.

##### 4.1. Noise Reduction Performance Analysis

To assess the noise reduction performance, a simulation comparison was conducted. The tested signal was a combination of two sinusoids with signal frequency  $f_1 = 100$  Hz and  $f_2 = 180$  Hz. The ambient noise was simulated by Gaussian noise. The sampling frequency was  $f_s = 1$  kHz, while the data length was  $N = 3000$  points to better reveal its output performance.

A comparison of the noise reduction performance is shown in Figure 4. The input SNR was set as  $-5$  dB. In Figure 4a,b, two narrowband line spectral signatures can be seen submerged in the background noise. By utilizing the convolution method (refer to  $p * p$ ), the results in the time and frequency domains are shown in Figure 4c. From the corresponding lofargram in Figure 4d, it is possible to clearly see the improvement in  $f_1$  and  $f_2$ , which reveals the effectiveness in terms of improved SNRI performance. The matched filtering (refer to  $p * s$ ) results are illustrated in Figure 4e,f, where it can be seen that superior filtering performance is achieved. A comparison of the normalized power spectrum density (PSD) of the input and output with the Welch method are further illustrated in Figure 5. As the noise reduction performance of both MF and COV are effective, we can expect good vector acoustic DOA estimation performance with both and better preprocessing with MF. Note that the algorithm for convolution preprocessing is simple, with  $N(N + 1) - 1$  times multiplier calculations and  $N(N - 1) - 1$  times add calculations. The computational complexity is low, and is related to the data length  $N$ . In this paper, the simulation was conducted in MATLAB with the 'conv' function. The runtime was recorded in Matlab R2019b on a platform configured with the following parameters: Intel i5, 3.2-GHz Quad Core processor, 8 GB memory, and a 64-bit Windows 10 operating system. The average runtime for 'COV' with ten runs was 0.000452 s.

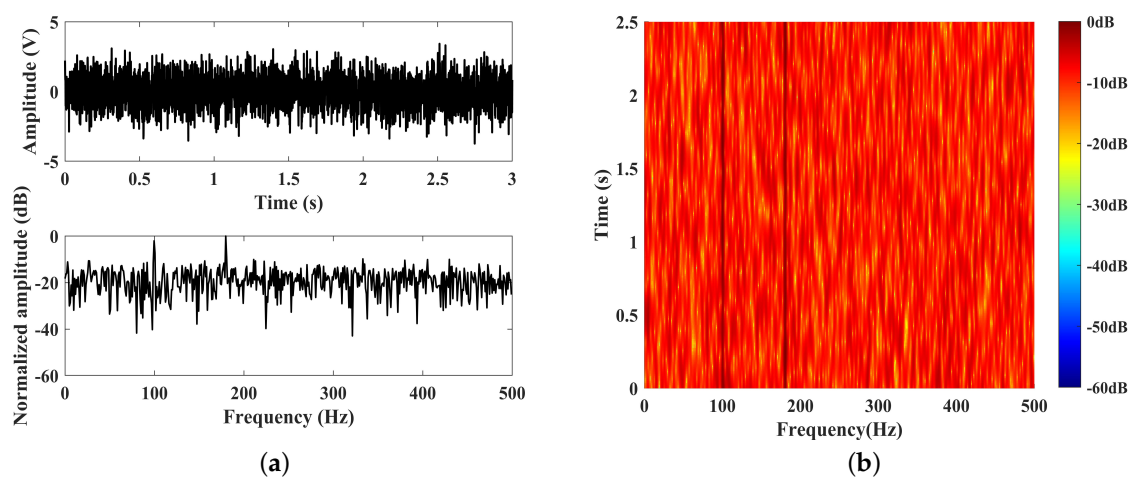
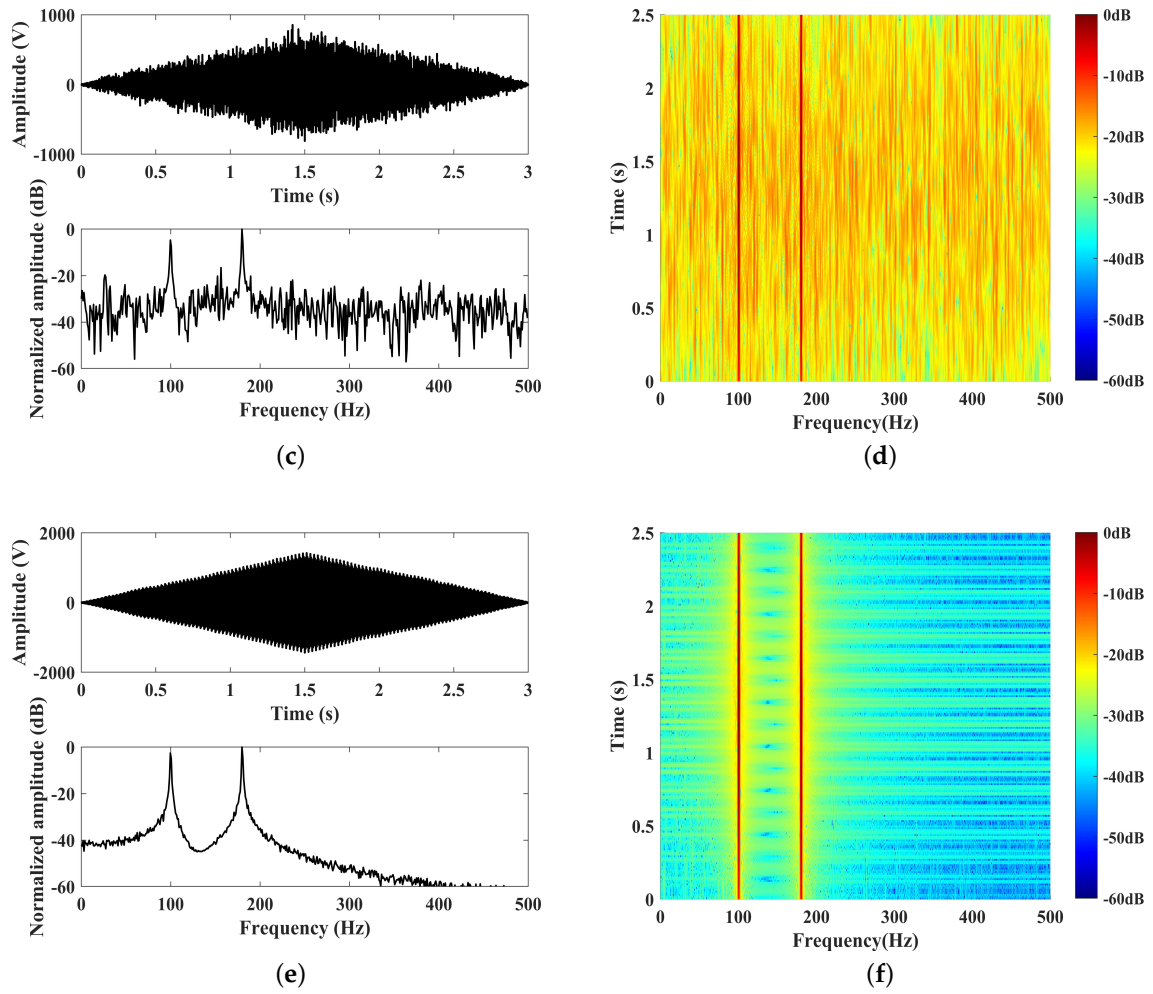
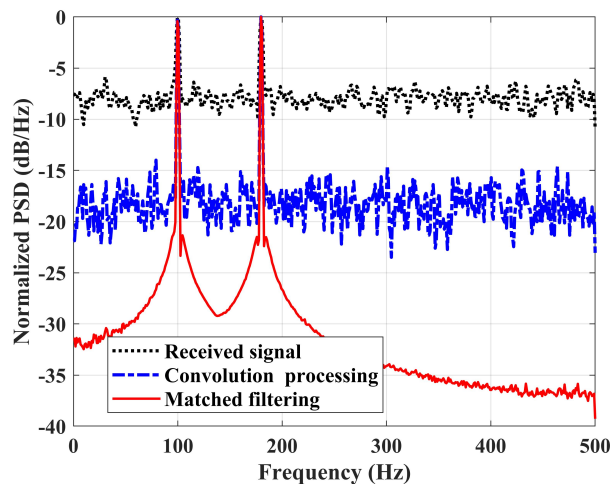


Figure 4. Cont.



**Figure 4.** Comparison of noise reduction performance: (a) noisy received signal; (b) lofargram of the noisy received signal; (c) convolution processed signal; (d) lofargram of the convolution processed signal; (e) matched filtering processed signal; (f) lofargram of the matched filtering processed signal.



**Figure 5.** Comparison of the normalized power spectrum density (PSD) with the Welch method for the noisy received signal, convolution processed signal, and matched filtering processed signal.

#### 4.2. Vector DOA Estimation Performance Analysis

To verify the effectiveness of the COV and MF preprocessing method for vector acoustic DOA estimation, the estimated mean error (ME) and root mean square error (RMSE) of the azimuth angle were evaluated with the classical MUSIC, AAIM, and CAIM methods. In the remainder of this paper, MUSIC<sub>COV</sub>, AAIM<sub>COV</sub>, and CAIM<sub>COV</sub> denote the classical vector DOA estimation methods with COV preprocessing, while MUSIC<sub>MF</sub>, AAIM<sub>MF</sub>, and CAIM<sub>MF</sub> denote MF preprocessing. Because the SNRs of UAVS channels are different, the P channel is adopted for reference. The target source azimuth was simulated as 30°, and the SNR of the signal was varied from -30 dB to 0 dB to verify its performance, especially under low SNR conditions. The signal length  $N$  was set as 1000 points.

The results are shown in Figure 6, with every data point the averaged of 2000 times. It is clear that the vector acoustic estimation performance can be effectively improved by MUSIC<sub>COV</sub>, AAIM<sub>COV</sub>, and CAIM<sub>COV</sub>. By utilizing MF preprocessing, the results of MUSIC<sub>MF</sub>, AAIM<sub>MF</sub>, and CAIM<sub>MF</sub> are superior, which can be regarded as the upper bound of the convolution-based single vector acoustic preprocessing methods. In view of the improvement in performance, the utilization of COV preprocessing is more effective for the MUSIC and AAIM methods than for the CAIM method. This means that the proposed COV preprocessing is more effective for vector acoustic DOA estimation methods subjected to time domain signals. As shown in Figure 6a, within 2° estimation error, the ME performance of the MUSIC, AAIM, and CAIM methods can be improved by around 3 dB, 4 dB, and 1 dB, respectively. Note that the analysis of ME performance can make sense for postprocessing methods of vector acoustic DOA such as particle filtering, histograms, etc. [27–29]. The RMSE performance results are shown in Figure 6b. It can be seen that within 5° estimation error, the RMSE performance of the MUSIC<sub>COV</sub>, AAIM<sub>COV</sub>, and CAIM<sub>COV</sub> methods can be consistently improved, which reveals the effectiveness of the proposed COV preprocessing.

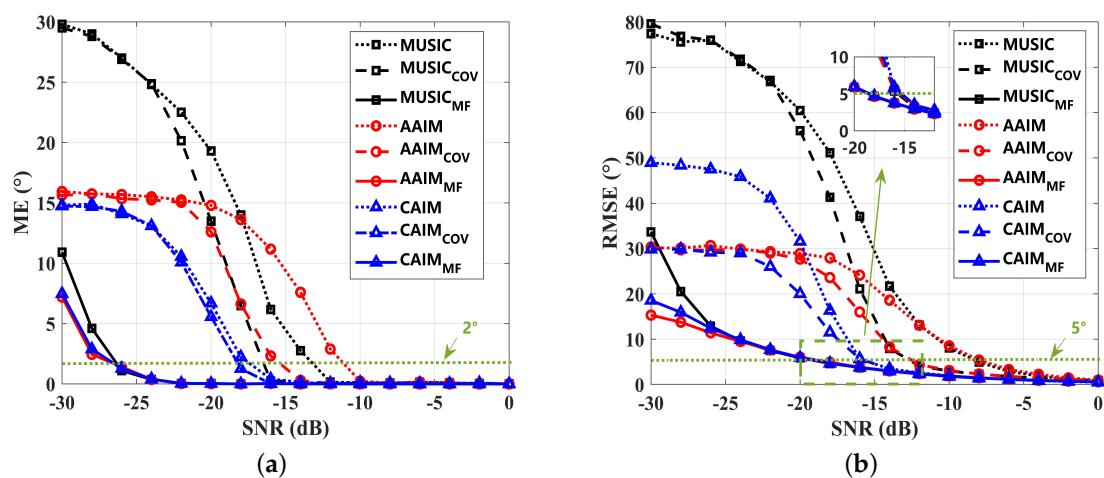


**Figure 6.** Performance comparison of different vector acoustic DOA estimation methods with COV preprocessing and MF preprocessing in terms of (a) mean error (ME) and (b) root mean square error (RMSE).

## 5. Experimental Verification

### 5.1. Experiment Description

To better reveal the practical application performance, a set of sea data was adopted from an experiment conducted in the South China Sea. In this experiment, a single UAVS that was installed on a deep-sea buoy and deployed at 1825 meters depth, as shown in Figure 7a. The sampling rate was  $f_s = 1$  kHz. As the line signatures are known as a set of narrow band discrete spectral components, a low frequency broadband sound source (UW350) was utilized to set the periodic signal frequency with 170 Hz and 270 Hz. The UW350 was deployed at three locations, named  $V_1$ ,  $V_2$ , and  $V_3$ , for different distances;

the relative distance to the UAVS and the true azimuth are provided as referenced to the measured GPS data. The detailed experimental layout parameters are shown in Table 1.

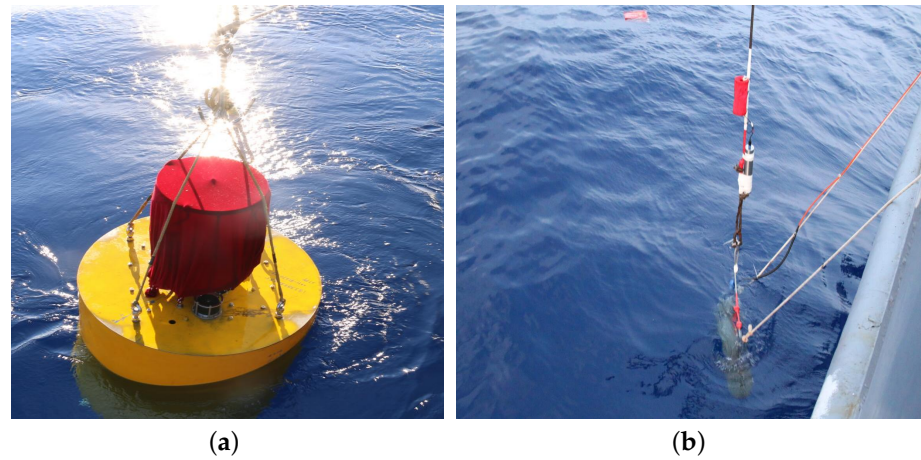


**Figure 7.** Sea experiment: (a) deep-sea buoy with a single UAVS and (b) deployment of the UW350 low-frequency broadband sound source.

**Table 1.** The experimental layout parameters.

Location	Longitude	Latitude	Layout Depth	Relative Distance (UAVS)	Ture Azimuth
UAVS	19° 24.30400'	115° 10.30700'	1825 m	0	0
$V_1$	19° 22.23300'	115° 11.56100'	96 m	4.42 km	189.74°
$V_2$	19° 27.18400'	115° 8.71600'	96 m	6.02 km	7.01°
$V_3$	19° 17.40600'	115° 14.16000'	96 m	14.44 km	187.30°

### 5.2. Vector Acoustic DOA Estimation Performance Analysis

The received signals of  $V_1$ ,  $V_2$ , and  $V_3$  and the corresponding COV preprocessing results are provided in Figures 8–10. A bandpass filter [150 Hz, 300 Hz] was utilized before COV preprocessing. The  $V_1$  point was about 4.42 km to the UAVS, which was the nearest. The ocean background noise was varied with time, with impulsive interference in about a 10 s period. The SNR of the  $p$  channel was the best overall, allowing us to clearly distinguish the signal frequencies of 170 Hz and 270 Hz in the time–frequency domain, as shown in Figure 8.

By utilizing our proposed COV preprocessing method, the signatures could be more clearly seen with certain denoising performance, with the results for the 270 Hz signal being better. For the longer-distance circumstances, as shown in Figures 9 and 10, the results for the 270 Hz signal are better as well. This is due to the higher level of ocean ambient noise in lower frequency bands. The ME and RMSE of the vector acoustic DOA estimation results corresponding to the different distances of the UW350 signals with MUSIC, AAIM, CAIM, MUSIC<sub>COV</sub>, AAIM<sub>COV</sub>, and CAIM<sub>COV</sub> are compared and listed in Table 2. Every data point was obtained from ten independent estimation results. It can be seen that the estimation error of the classical MUSIC, AAIM, and CAIM is larger than 4°. When using our proposed COV preprocessing, however, the estimation error is greatly decreased, revealing improved performance. Among MUSIC<sub>COV</sub>, AAIM<sub>COV</sub>, and CAIM<sub>COV</sub>, we found that CAIM<sub>COV</sub> performed the best, which is in accordance with the simulated results. In addition, the estimation performance for the 270 Hz signal was better than for the 170 Hz signal. This is due to the complex noise background in lower frequency bands, where the ocean background noise corresponding to 170 Hz is more complicated.

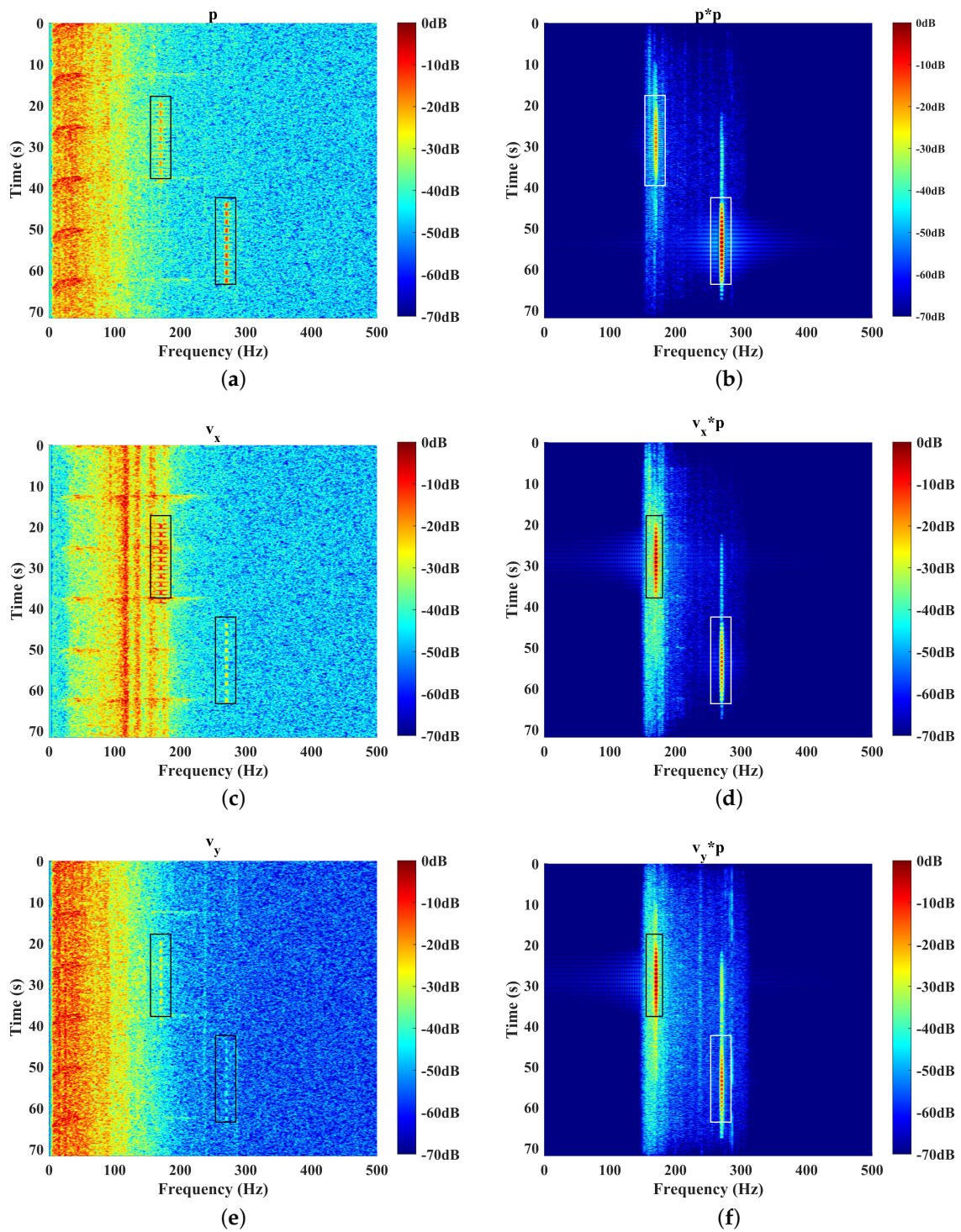


**Figure 8.** Comparison of COV preprocessing for vector  $p$ ,  $v_x$ , and  $v_y$  channels of  $V_1$  data with reference  $p$  channel signal: (a) lofargram of the  $p$  channel signal; (b) lofargram of the COV processed  $p$  channel ( $p * p$ ); (c) lofargram of the  $v_x$  channel signal; (d) lofargram of the COV processed  $v_x$  channel ( $v_x * p$ ); (e) lofargram of the  $v_y$  channel signal; (f) lofargram of the COV processed  $v_y$  channel ( $v_y * p$ ).

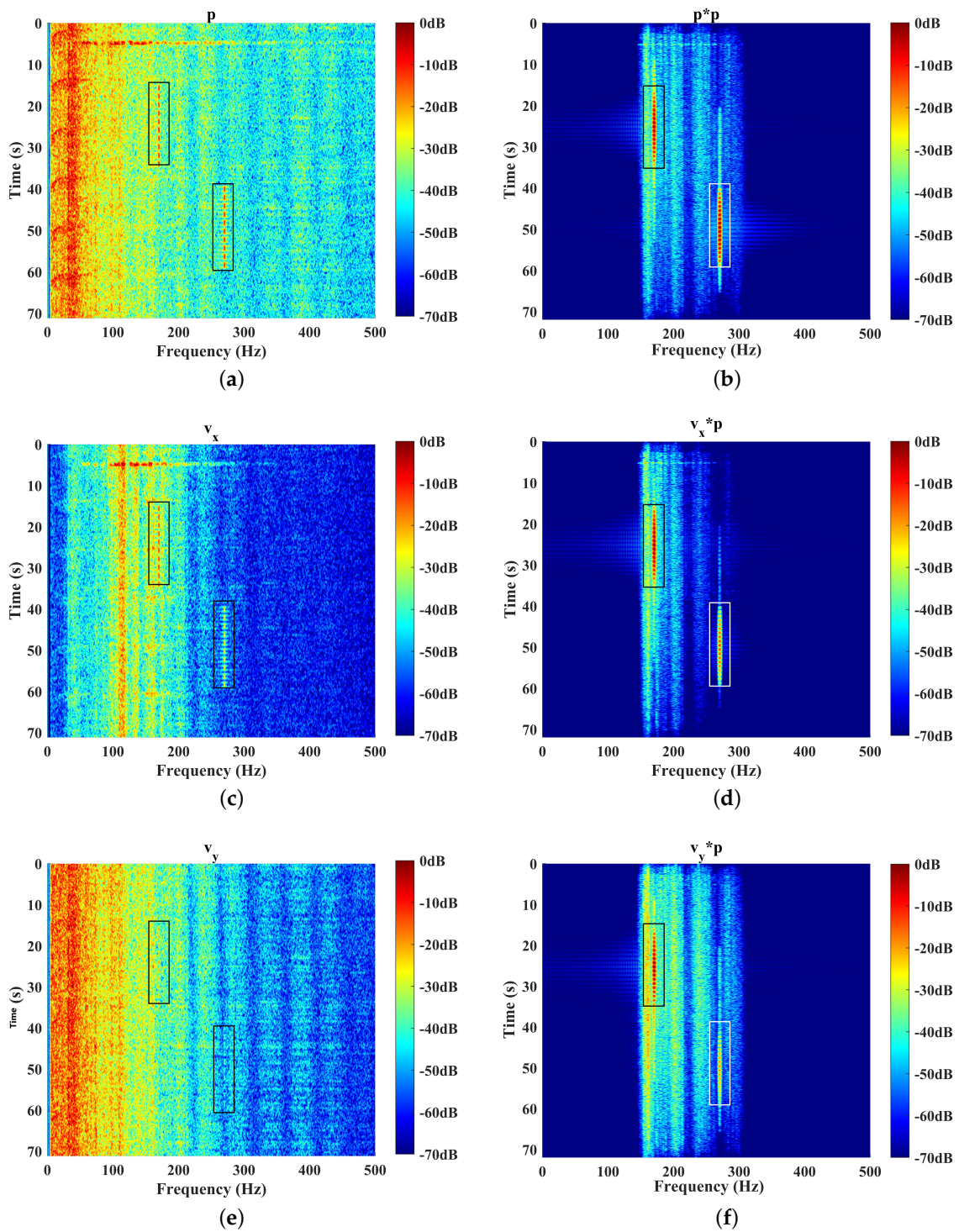


**Figure 9.** Comparison of COV preprocessing for vector  $p$ ,  $v_x$ , and  $v_y$  channels of  $V_2$  data with reference  $p$  channel signal: (a) lofargram of the  $p$  channel signal; (b) lofargram of the COV processed  $p$  channel ( $p * p$ ); (c) lofargram of the  $v_x$  channel signal; (d) lofargram of the COV processed  $v_x$  channel ( $v_x * p$ ); (e) lofargram of the  $v_y$  channel signal; (f) lofargram of the COV processed  $v_y$  channel ( $v_y * p$ ).

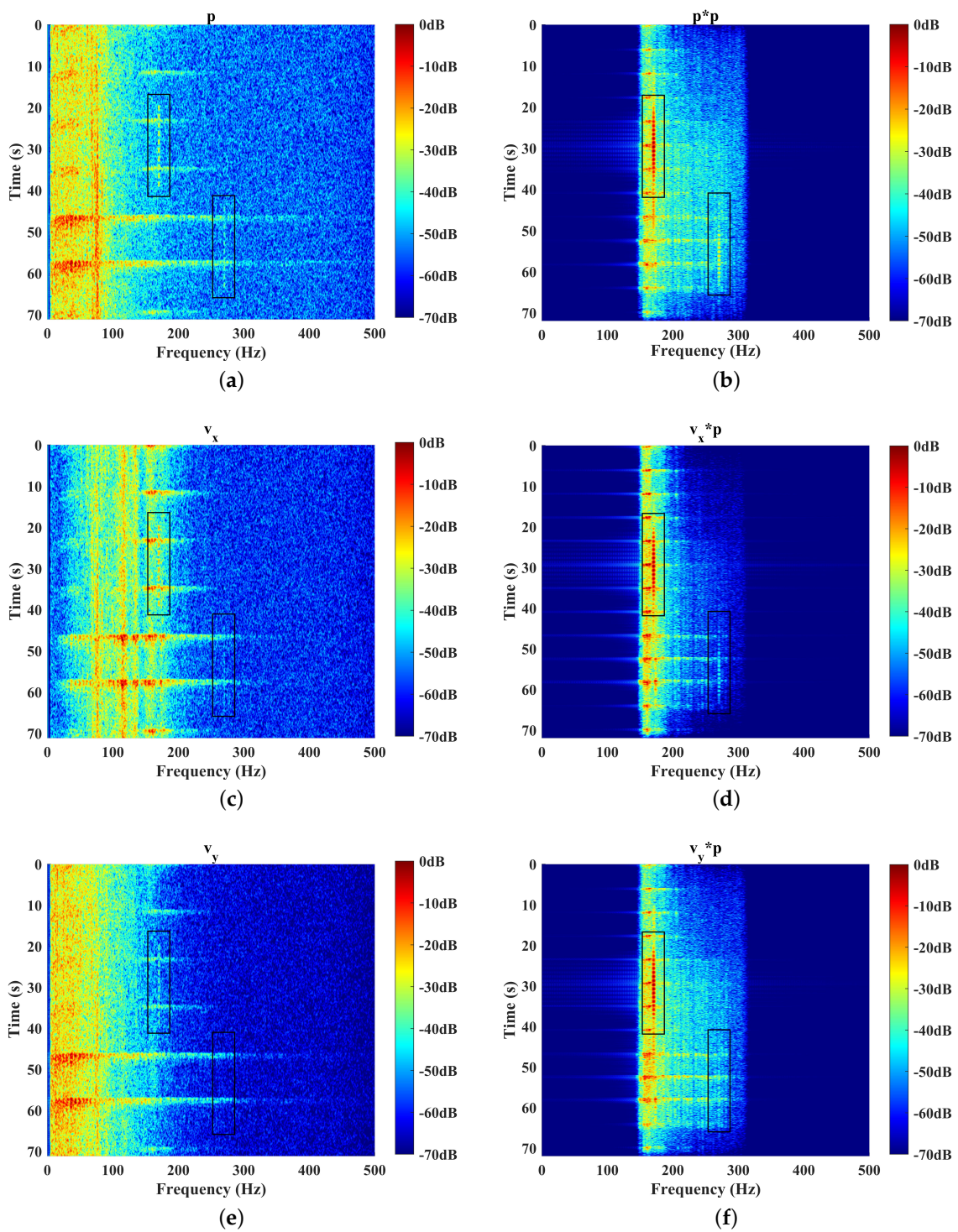


**Figure 10.** Comparison of COV preprocessing for vector  $p$ ,  $v_x$ , and  $v_y$  channels of  $V_3$  data with reference  $p$  channel signal: (a) lofargram of the  $p$  channel signal; (b) lofargram of the COV processed  $p$  channel ( $p * p$ ); (c) lofargram of the  $v_x$  channel signal; (d) lofargram of the COV processed  $v_x$  channel ( $v_x * p$ ); (e) lofargram of the  $v_y$  channel signal; (f) lofargram of the COV processed  $v_y$  channel ( $v_y * p$ ).

**Table 2.** Estimated mean error (ME) and root mean square error (RMSE) of the azimuth angle for received UW350 signals under different distances.

Signal	Error	MUSIC	AAIM	CAIM	MUSIC <sub>COV</sub>	AAIM <sub>COV</sub>	CAIM <sub>COV</sub>
$V_1$ (270 Hz)	ME	2.43°	1.82°	1.29°	1.24°	1.01°	<b>0.85°</b>
	RMSE	5.54°	4.80°	4.16°	2.24°	2.01°	<b>1.43°</b>
$V_1$ (170 Hz)	ME	9.74°	7.51°	5.19°	3.24°	2.33°	<b>1.83°</b>
	RMSE	15.74°	12.51°	11.19°	6.24°	4.38°	<b>3.62°</b>
$V_2$ (270 Hz)	ME	1.01°	0.98°	0.67°	0.59°	0.56°	<b>0.43°</b>
	RMSE	2.48°	1.94°	1.56°	1.83°	1.25°	<b>1.04°</b>
$V_2$ (170 Hz)	ME	9.04°	7.21°	5.35°	3.51°	2.38°	<b>1.16°</b>
	RMSE	14.01°	11.12°	10.39°	5.14°	3.82°	<b>2.61°</b>
$V_3$ (270 Hz)	ME	14.30°	10.03°	8.87°	11.32°	9.36°	<b>7.37°</b>
	RMSE	33.60°	18.00°	17.28°	19.32°	15.37°	<b>12.63°</b>
$V_3$ (170 Hz)	ME	31.25°	22.84°	17.55°	27.65°	14.51°	<b>11.32°</b>
	RMSE	87.30°	28.84°	36.52°	57.65°	25.14°	<b>23.28°</b>

The estimation error for the  $V_2$  point data can be better than for  $V_1$ . Although the relative distance to the UAVS is larger, the background noise is more stationary, as shown in Figure 9. This indicates that the non-Gaussian and impulsive properties of the noise greatly affect the estimation performance. For  $V_3$  point data, the relative distance is about 14.44km. It can be seen that the SNR of the received signal is lower when the signals to be detected are weak, as shown in Figure 10. In this circumstance, the overall estimation error is increased; MUSIC and MUSIC<sub>COV</sub> see loss of performance, with an extremely large error for the 170Hz signal. The RMSEs for CAIM<sub>COV</sub> corresponding to different distances are all optimal. This reveals that our proposed COV preprocessing method could be effective in dealing with weak signals with impulsive background noise.

According to the aforementioned analyses, our proposed COV preprocessing method can effectively enhance vector acoustic DOA estimation performance, demonstrating its potential for practical application in single acoustic vector DOA estimation, especially under lower SNR conditions and complex noisy circumstances. In view of the superior performance of the MF preprocessing method, COV preprocessing could have room for improvement. As discussed in Section 3, the generalized vector acoustic preprocessing model can be described as seeking “to achieve an improved denoising performance in the constraint of equivalent amplitude gain and phase response.” Our proposed COV and MF basically satisfy this constraint; however, without loss of generality, we think that there are other approaches that could achieve the constraints as well. This represents important guidance for future research work.

## 6. Conclusions

In this paper, a novel convolution (COV)-based single-vector acoustic preprocessing method is proposed on the basis of the single-vector acoustic preprocessing model. The proposed approach can naturally guarantee the principle of vector preprocessing in order to achieve improved denoising performance under the constraint of equivalent amplitude gain and phase response. Numerical analyses conducted with the classical MUSIC, AAIM, and CAIM methods demonstrate the effectiveness of our proposed COV preprocessing method for both vector array signal processing-based and intensity-based methods. Experimental verification conducted in the South China Sea further verifies its effectiveness for practical application. In addition, its the upper bound with matched filtering (MF) preprocessing is provided under consideration of optimal linear signal processing for weak signal detection under Gaussian noise. In view of the linearity principle of preprocessing, the single-vector acoustic preprocessing model allows for a new point of view on preprocessing restrictions for vector acoustic DOA estimation, and can represent a breakthrough innovation in guidance for underwater acoustic remote sensing with vector sensors in the future. In

recent years, deep learning has led to rapid development in a variety of research fields. For vector acoustic signal processing, deep learning has already been adopted to improve AVS-DOA estimation performance, although there is a lack of theoretical guidance. We think that our proposed method can be an important guide to learning tasks, especially in determining better loss function design. This work will be further studied in the future.

**Author Contributions:** H.D.: conceptualization, methodology, software, validation, writing—original draft preparation. J.S.: methodology, data curation. Z.Z.: data curation, writing—review and editing. S.L.: data curation, writing—review and editing. All authors have read and agreed to the published version of the manuscript.

**Funding:** This work was supported by the National Natural Science Foundation of China (Grant No. 62201439, 62031021, 62203343), the China Postdoctoral Science Foundation (Grant No. 2022M722493), the Fundamental Research Funds for the Central Universities (Grant No. XJSJ23026), and the Postdoctoral Research Project of Shanxi Province (Grant No. 2023BSHEDZZ174).

**Data Availability Statement:** Data sharing is not applicable to this article. The data presented in this study are available on request from the corresponding author.

**Conflicts of Interest:** The authors declare no conflicts of interest. The founding sponsors had no role in the design of the study or in the decision to publish the results.

## References

1. Blomberg, A.E.A.; Austeng, A.; Hansen, R.E.; Synnes, S.A.V. Improving sonar performance in shallow water using adaptive beamforming. *IEEE J. Ocean. Eng.* **2013**, *38*, 297–307. [\[CrossRef\]](#)
2. Cao, J.; Liu, J.; Wang, J.; Lai, X. Acoustic vector sensor: Reviews and future perspectives. *IET Signal Process.* **2016**, *11*, 1–9. [\[CrossRef\]](#)
3. Wu, K.; Reju, V.G.; Khong, A.W. Multisource DOA estimation in a reverberant environment using a single acoustic vector sensor. *IEEE/ACM Trans. Audio Speech Lang. Process.* **2018**, *26*, 1848–1859. [\[CrossRef\]](#)
4. Stinco, P.; Tesei, A.; Dreo, R.; Micheli, M. Detection of envelope modulation and direction of arrival estimation of multiple noise sources with an acoustic vector sensor. *J. Acoust. Soc. Am.* **2021**, *149*, 1596–1608. [\[CrossRef\]](#) [\[PubMed\]](#)
5. Nehorai, A.; Paldi, E. Acoustic vector-sensor array processing. *IEEE Trans. Signal Process.* **1994**, *42*, 2481–2491. [\[CrossRef\]](#)
6. Wong, K.T.; Zoltowski, M.D. Uni-vector-sensor ESPRIT for multisource azimuth, elevation, and polarization estimation. *IEEE Trans. Antennas Propag.* **1997**, *45*, 1467–1474. [\[CrossRef\]](#)
7. Miron, S.; Le Bihan, N.; Mars, J.I. Quaternion-MUSIC for vector-sensor array processing. *IEEE Trans. Signal Process.* **2006**, *54*, 1218–1229. [\[CrossRef\]](#)
8. Han, K.; Nehorai, A. Nested vector-sensor array processing via tensor modeling. *IEEE Trans. Signal Process.* **2014**, *62*, 2542–2553. [\[CrossRef\]](#)
9. Najeem, S.; Kiran, K.; Malarkodi, A.; Latha, G. Open lake experiment for direction of arrival estimation using acoustic vector sensor array. *Appl. Acoust.* **2017**, *119*, 94–100. [\[CrossRef\]](#)
10. Weiss, A. Blind direction-of-arrival estimation in acoustic vector-sensor arrays via tensor decomposition and Kullback-Leibler divergence covariance fitting. *IEEE Trans. Signal Process.* **2020**, *69*, 531–545. [\[CrossRef\]](#)
11. Dreo, R.; Trabattoni, A.; Stinco, P.; Micheli, M.; Tesei, A. Detection and localization of multiple ships using acoustic vector sensors on buoyancy gliders: Practical design considerations and experimental verifications. *IEEE J. Ocean. Eng.* **2022**, *48*, 577–591. [\[CrossRef\]](#)
12. Zhang, R.; Zhou, S.; Qi, Y.; Liang, Y.; Sui, Y. Characteristics of very-low-frequency pulse acoustic fields measured by vector sensor and ocean bottom seismometer in shallow water. *J. Acoust. Soc. Am.* **2018**, *144*, 1916. [\[CrossRef\]](#)
13. Silvia, M.T.; Richards, R.T. A theoretical and experimental investigation of low-frequency acoustic vector sensors. In Proceedings of the OCEANS'02 MTS/IEEE, Biloxi, MI, USA, 29–31 October 2002; IEEE: Piscataway, NJ, USA, 2002; Volume 3, pp. 1886–1897.
14. Thode, A.; Skinner, J.; Scott, P.; Roswell, J.; Straley, J.; Folkert, K. Tracking sperm whales with a towed acoustic vector sensor. *J. Acoust. Soc. Am.* **2010**, *128*, 2681–2694. [\[CrossRef\]](#) [\[PubMed\]](#)
15. Tichavsky, P.; Wong, K.T.; Zoltowski, M.D. Near-field/far-field azimuth and elevation angle estimation using a single vector hydrophone. *IEEE Trans. Signal Process.* **2001**, *49*, 2498–2510. [\[CrossRef\]](#)
16. Zhao, A.; Ma, L.; Hui, J.; Zeng, C.; Bi, X. Open-lake experimental investigation of azimuth angle estimation using a single acoustic vector sensor. *J. Sensors* **2018**, *2018*, 4324902. [\[CrossRef\]](#)
17. Bereketi, A.; Guldogan, M.B.; Kolcak, T.; Gudu, T.; Avsar, A.L. Experimental results for direction of arrival estimation with a single acoustic vector sensor in shallow water. *J. Sensors* **2015**, *2015*, 401353. [\[CrossRef\]](#)
18. Zhao, A.; Ma, L.; Ma, X.; Hui, J. An improved azimuth angle estimation method with a single acoustic vector sensor based on an active sonar detection system. *Sensors* **2017**, *17*, 412. [\[CrossRef\]](#)

19. Wu, Y.I.; Wong, K.T.; Yuan, X.; Lau, S.K.; Tang, S.K. A directionally tunable but frequency-invariant beamformer on an acoustic velocity-sensor triad to enhance speech perception. *J. Acoust. Soc. Am.* **2012**, *131*, 3891–3902. [[CrossRef](#)]
20. Thode, A.M.; Kim, K.H.; Norman, R.G.; Blackwell, S.B.; Greene, C.R.J. Acoustic vector sensor beamforming reduces masking from underwater industrial noise during passive monitoring. *J. Acoust. Soc. Am.* **2016**, *139*, EL105–EL111. [[CrossRef](#)] [[PubMed](#)]
21. Suo, J.; Dong, H.; Shen, X.; Wang, H. Bistable stochastic resonance with linear amplitude response enhanced vector DOA estimation under low SNR conditions. *Chaos Solitons Fractals* **2020**, *136*, 109825. [[CrossRef](#)]
22. Terracciano, D.S.; Costanzi, R.; Manzari, V.; Stifani, M.; Caiti, A. Passive bearing estimation using a 2-D acoustic vector sensor mounted on a hybrid autonomous underwater vehicle. *IEEE J. Ocean. Eng.* **2022**, *47*, 799–814. [[CrossRef](#)]
23. Suo, J.; Wang, H.; Dong, H.; Shen, X.; Yan, Y.; Zhang, H. Single acoustic vector sensor DOA enhanced by unsaturated bistable stochastic resonance with linear amplitude response constrained. *Appl. Acoust.* **2023**, *214*, 109695. [[CrossRef](#)]
24. Hochwald, B.; Nehorai, A. Identifiability in array processing models with vector-sensor applications. *IEEE Trans. Signal Process.* **1996**, *44*, 83–95. [[CrossRef](#)]
25. Agarwal, A.; Agrawal, M.; Kumar, A. Higher-order-statistics-based direction-of-arrival estimation of multiple wideband sources with single acoustic vector sensor. *IEEE J. Ocean. Eng.* **2019**, *45*, 1439–1449. [[CrossRef](#)]
26. Zhang, J.; Xu, X.; Chen, Z.; Bao, M.; Zhang, X.P.; Yang, J. High-resolution DOA estimation algorithm for a single acoustic vector sensor at low SNR. *IEEE Trans. Signal Process.* **2020**, *68*, 6142–6158. [[CrossRef](#)]
27. Zhong, X.; Premkumar, A.B. Particle filtering approaches for multiple acoustic source detection and 2-D direction of arrival estimation using a single acoustic vector sensor. *IEEE Trans. Signal Process.* **2012**, *60*, 4719–4733. [[CrossRef](#)]
28. Gunes, A.; Guldogan, M.B. Joint underwater target detection and tracking with the Bernoulli filter using an acoustic vector sensor. *Digit. Signal Process.* **2016**, *48*, 246–258. [[CrossRef](#)]
29. Chen, Y.; Wang, W.; Wang, Z.; Xia, B. A source counting method using acoustic vector sensor based on sparse modeling of DOA histogram. *IEEE Signal Process. Lett.* **2019**, *26*, 69–73. [[CrossRef](#)]
30. Wang, D.; Zou, Y.; Wang, W. Learning soft mask with DNN and DNN-SVM for multi-speaker DOA estimation using an acoustic vector sensor. *J. Frankl. Inst.* **2018**, *355*, 1692–1709. [[CrossRef](#)]
31. Cao, H.; Wang, W.; Su, L.; Ni, H.; Gerstoft, P.; Ren, Q.; Ma, L. Deep transfer learning for underwater direction of arrival using one vector sensor. *J. Acoust. Soc. Am.* **2021**, *149*, 1699–1711. [[CrossRef](#)]
32. Sun, G.; Yang, D.; Shi, G. Spatial correlation coefficients of acoustic pressure and particle velocity based on vector hydrophone. *Acta Acust.* **2003**, *28*, 509–513.
33. Ross, D. *Mechanics of Underwater Noise*; Pergamon Press: Los Altos, CA, USA, 1976; pp. 272–280.
34. Dong, H.; Wang, H.; Shen, X.; He, K. Parameter matched stochastic resonance with damping for passive sonar detection. *J. Sound Vib.* **2019**, *458*, 479–496. [[CrossRef](#)]

**Disclaimer/Publisher’s Note:** The statements, opinions and data contained in all publications are solely those of the individual author(s) and contributor(s) and not of MDPI and/or the editor(s). MDPI and/or the editor(s) disclaim responsibility for any injury to people or property resulting from any ideas, methods, instructions or products referred to in the content.